International Communications in Heat and Mass Transfer 56 (2014) 146–151

Contents lists available at ScienceDirect

International Communications in Heat and Mass Transfer

journal homepage: www.elsevier.com/locate/ichmt

Numerical simulation of nanostructured thermoelectric generator considering surface to surrounding convection ☆

Ronil Rabari, Shohel Mahmud *, Animesh Dutta

School of Engineering, University of Guelph, Guelph, Ontario, Canada

ARTICLE INFO

Available online 14 June 2014

Keywords:
Thermoelectric
Convection heat loss
Numerical simulation
Nanostructuring

ABSTRACT

Thermoelectric systems (TE) can directly convert heat to electricity and vice-versa by using semiconductor materials. Therefore, coupling between heat transfer and electric field potential is important to predict the performance of thermoelectric generator (TEG) systems. This paper develops a general two-dimensional numerical model of a TEG system using nanostructured thermoelectric semiconductor materials. A TEG with *p*-type nanostructured material of Bismuth Antimony Telluride (*BiSbTe*) and *n*-type Bismuth Telluride (Bi_2Te_3) with 0.1 vol.% Silicon Carbide (*SiC*) nanoparticles is considered for performance evaluations. Coupled TE equations with temperature dependant transport properties are used after incorporating Fourier heat conduction, Joule heating, Seebeck effect, Peltier effect, and Thomson effect. The effects of temperature difference between the hot and cold junctions and surface to surrounding convective on different output parameters (e.g., thermal and electric fields, power generation, thermal efficiency, and current) are studied. Selected results obtained from current numerical analysis are compared with the results obtained from analytical model available in the literature. There is a good agreement between the numerical and analytical results. The numerical results show that as temperature difference increases output power and amount of current generated increase. Moreover, it is quite apparent that convective boundary condition deteriorates the performance of TEG.

1. Introduction

The research and development in nanostructured TE systems have gathered considerable attention due to their potential applications in direct electricity generation, refrigeration, and air-conditioning. TE systems can largely be classified as thermoelectric generator (TEG) and thermoelectric cooler (TEC). The TEG converts heat into electricity and TEC converts electricity into heating/cooling based on Seebeck and Peltier effects, respectively. TE systems are solid state heat engines/refrigerators which are robust, silent, compact, and environment friendly. TE systems are made up of numbers of *p*-type and *n*-type semiconductor elements connected electrically in series and thermally in parallel. The TEC has a wide range of applications; for example, electronic cooling, laser diode cooling, military garment, laboratory cold plates, and automobile seat cooler. In a similar manner, TEG has various applications in military, deep space vehicles, remote power sources for inhabitable places, solar and waste heat power generator. Liquid cooling of CPU using TE was proposed and experimentally investigated considering different material and size of the heat sinks [1]. Huang et al. [2] discussed TE cooling of electronic equipment experimentally and analytically. The results determined that the integration of water-cooling with TE is helpful to increase the performance of electronic equipment. In order to address the site specific on-demand cooling of hot spot in microprocessor [3], a numerical simulation that includes heat spreader, thermal interface material, chip, and nine TECs was carried out considering steady state and transient analysis. Sullivan et al. [3] concluded that transient cooling with square root current pulse is most effective with 10 °C cooling. Wang [4] proposed and investigated experimentally the TEG using waste heat of the Light-Emitting Diodes. Results reported by Wang [4] investigated power output of TEG using waste heat of the Light-Emitting Diodes (LED). Experiments of Wang [4] showed 160 mW of power output from TEG with 6 W of input power to LED. Recently, Hsiao et al. [5] studied the performance of TE modules as a waste heat recovery tool from an automobile engine using a one-dimensional thermal resistance model and compared their model with experimental data. Results [5] showed that the performance of a TE module on the exhaust pipe performs better compared to a TE module on the radiator system. Rezania et al. [6] studied the effect of cooling power on the performance of a TEG. Rezania et al. [6] determined the optimum coolant flow rate for maximum power output for the TEG. For example, temperature difference of 10 K gives maximum power output of 0.035 W with coolant flow rate of 0.07 l/min [6]. One-dimensional analytical solutions of conventional, composite, and integrated TEG were carried out by Reddy et al. [7] considering adiabatic and convective side wall conditions. Regardless of TEG design, an increment in the hot side

☆ Communicated by W.J. Minkowycz.

* Corresponding author.
E-mail address: smahmud@uoguelph.ca (S. Mahmud).

http://dx.doi.org/10.1016/j.icheatmasstransfer.2014.06.006
0735-1933/

Nomenclature

C	specific heat capacity (kJ/kg K)
D	electric flux density vector (C/m^2)
E	electric field intensity vector (N/C)
e	electron charge (1.60×10^{-19}C)
h	convection heat transfer coefficient (W/m^{2}K)
H	height of TE leg (m)
I	current (A)
J	electric current density (A/m^2)
k	Boltzmann constant (JK–1)
L	length (m)
L_o	Lorentz number (V^{2}K^{-2})
R	resistance (Ω)
q	heat (W)
q·	heat generation rate per unit volume (W/m^3)
Q	heat (W)
t	time (S)
T	temperature (K)
W	width of the TE leg (m)
x	coordinate (m)
y	coordinate (m)
ZT	dimensionless figure of merit
p	p-type semiconductor material
n	n-type semiconductor material

Greek symbols

α	Seebeck coefficient (V/K)
ρ	density (kg/m^3)
λ	thermal conductivity (W/mK)
σ	electrical conductivity (S/m)
ϕ	electric scalar potential (V)
n	thermal efficiency
ε	dielectric permittivity matrix (F/m)

Subscripts

C	cold surface
conv	convection
E	electronic
g	gap
H	hot surface
L	external load
L	lattice
p	p-type material
n	n-type material

temperature enhances the performance of TEG systems [7]. Reddy et al. [7] concluded that composites and integrated TEG extracts more heat compared to conventional TEG and reduces rare-element material usage. Gou et al. [8] investigated the performance of low temperature waste heat TEG using one-dimensional analytical simulations and experiments. They [8] concluded that in addition to increasing the waste heat temperature and number of modules in series, expanding the heat sink surface area and enhancing the cold side heat transfer in proper ranges can have dramatic effects on TEG's performance. A three dimensional numerical model of TEG applied to fluid power systems was developed by Chen et al. [9] and their numerical simulation performed with ANSYS showed fairly good match with experimental results. In addition to this, Chen et al. [9] concluded that convection heat transfer losses increase the heat input to TEG thus reducing the thermal efficiency of TEG. A three-dimensional coupled numerical simulation of integrated TE device was carried out by Reddy et al. [10] to check the effects of Reynolds number and fluid temperature on performance of an integrated TEG system. Reddy et al. [10] found that higher Reynolds number enhances heat transfer and thus leads to higher power output of TEG. Zhou et al. [11] developed simple and coupled field model with the former considering Navier–Stokes and energy equations with continuity equation and latter with different TE effects such as Seebeck, Peltier, and Thomson effect. Zhou et al. [11] reported overall TEG efficiency of 3.5% with temperature difference of 80 K. Baranowski et al. [12] developed mathematical model for solar TEG which can provide analytical solutions of device efficiency with temperature dependant properties. They [12] also showed that considering currently available materials, total efficiency of 14.1% is possible with cold and hot side temperatures of 100 °C and 1000 °C, respectively. Baranowski et al. [12] also concluded that if figure of merit (ZT) reaches 2 then TEG efficiency of 25% can be obtained, for the cold and hot side temperatures of 100 °C and 1000 °C, respectively.

Altenkirch [13] introduced figure of merit, ZT as a parameter to classify different materials. The performance of TE materials are characterized by a dimensionless parameter 'figure of merit', $ZT = (\alpha^2\sigma/\lambda)T$, where α is the Seebeck coefficient, σ is the electrical conductivity, and λ is the thermal conductivity. The current ZT value of the best available TE materials is 1 at room temperature [14]. Slack [15] described that good TE materials need to have low thermal conductivity. In addition to this, Slack [15] described that the best TE material would behave as "Phonon Glass Electron Crystal (PGEC)"; that is, it would have thermal properties of glass like material and electrical properties of crystalline material. Recent advancements in the field of nanotechnology [14] have opened the door for further improvements of ZT for the TE materials. The expression of the figure of merit, $ZT = (\alpha^2\sigma/\lambda)\,T$, evidently indicates that one of the methods to increase figure of merit is to reduce the thermal conductivity of the TE material. Thermal conductivity is the sum of two contributions: electrons and hole transporting the heat (λ_E) and phonons traveling through the lattice (λ_L) [16]. The electronic part of thermal conductivity (λ_E) is related to the electrical conductivity as per the Wiedemann–Franz law [16] as shown in Eq. (1),

$$\lambda_E = L_o T\sigma \tag{1}$$

where, L_o is the Lorentz number and for metals it is equal to [16],

$$L_o = \frac{\pi^2 k^2}{3e^2} = 2.45 \times 10^{-8}\mathrm{V}^2\mathrm{K}^{-2} \tag{2}$$

where, k is the Boltzmann constant (1.38×10^{-23} JK^{-1}) [16] and e is the electron charge (1.60×10^{-19}C) [17]. The expression of the figure of merit can be written in terms of Lattice conductivity (λ_L) and electronic conductivity (λ_E) as shown below [16],

$$\mathrm{ZT} = \frac{\alpha^2}{L_o}\frac{\lambda_E}{\lambda_E + \lambda_L} \tag{3}$$

One method to enhance ZT is the inclusion of nanoparticles into the bulk TE materials which can lead to low lattice thermal conductivity [18]. Poudel et al. [19] achieved ZT value of 1.4 at 373K by hot-pressing of nanopowders of Bi_2Te_3 and Sb_2Te_3 under Argon (Ar) atmosphere. The enhanced ZT was due to the significant decrease in the lattice thermal conductivity of material. Zhao et al. [20] fabricated Bi_2Te_3 with various amounts of nano SiC particles using mechanical alloying and spark plasma sintering and tested the TE and mechanical properties. Their results showed an improvement in ZT from 0.99 to 1.04 with an inclusion of 0.1% vol.% SiC particles. Li et al. [21] obtained ZT of 1.43 for double-doped Co_4Sb_{12} skutterudites using Indium (In) and Cerium (Ce) doping. The attractive results achieved using nanotechnology has encouraged researchers to include nanoparticle-doped TE materials for various low potential heat recovery applications; for example, solar TEG and automobile exhaust heat recovery. Kraemer et al. [22] have proposed novel solar TEG with glass vacuum enclosure considering nanostructured TE materials.

The developed solar TEG achieved maximum efficiency of 4.6% with solar flux of 1000 W/m^2 condition. McEnaney et al. [23] developed a novel TEG. They [23] placed high performance nanostructured material in evacuated tube with selective absorber and achieved an efficiency of 5.2%. It is quite evident that nanostructured TE materials can increase the performance of TE systems.

It is quite clear from the above discussion that in future nanostructured TE materials will play a significant role as a direct energy conversion tool from low potential sources. It is necessary to understand the wide range of characteristic features of newly developed TE materials. Such characteristic features include heat transport and electric potential. The existing literature on the numerical simulation of nanostructured TEG is very limited. In this paper, performance of nanostructured TEG is evaluated using 2D numerical simulation. The temperature dependent thermophysical and electrical properties of nanostructured TE material, surface to surrounding convection heat transfer losses, and Thomson effect are included in the current model. The field plots of heat and current are presented with different convection heat transfer coefficients. Numerical results are compared with that of one dimensional analytical results in terms of current produced.

2. Mathematical model and boundary conditions

The two-dimensional schematic diagram of the TEG being investigated is shown in Fig. 1. The TEG is mainly comprised of two vertical *p*-type and *n*-type semiconductor legs connected electrically in series and thermally in parallel. Both legs are connected through an electrically conductive copper strip. Each leg has a cross-sectional area of $L \times W$, height of H, and separated by distance L_g as shown in Fig. 1. The Q_H and Q_C are amount of heat available at heat source and heat sink respectively. The Q_{conv} is convection heat loss through the side walls of the TEG. During the analysis following assumptions are made:

- TE materials are homogeneous and isotropic with temperature dependent properties.
- Contact resistances at interface of copper and TE materials are neglected.

In the TEG, the energy transport and current flow are governed by energy equation and continuity of current density as per below,

$$\rho\ C\frac{\partial T}{\partial t} + \nabla \cdot \mathbf{q} = \dot{q}_{gen} \tag{1}$$

where symbols ρ, C_p, T, $\mathbf{q}$, and $\dot{q}_{gen}$ represent material density, specific heat, temperature, heat generation rate per unit volume, and heat flux vector, respectively. The continuity of electric charge through the system must satisfy,

$$\nabla \cdot \left(\mathbf{J} + \frac{\partial \mathbf{D}}{\partial t}\right) = 0 \tag{2}$$

where $\mathbf{J}$ is the electric current density vector and $\mathbf{D}$ is the electric flux density vector, respectively. Eqs. (1) and (2) are coupled by the set of TE constitutive equations [24] as shown in Eqs. (3) and (4),

$$\mathbf{q} = T[\alpha] \cdot \mathbf{J} - [\lambda] \cdot \nabla T \tag{3}$$

$$\mathbf{J} = [\sigma] \cdot (\mathbf{E} - [\alpha] \cdot \nabla T) \tag{4}$$

where $[\alpha]$ is the Seebeck coefficient matrix, $[\lambda]$ is the thermal conductivity matrix, $[\sigma]$ is the electrical conductivity matrix, and $\mathbf{E}$ is the electric field intensity vector, respectively. $\mathbf{E}$ can be expressed as $-\nabla\phi$, where ϕ is the electric scalar potential [25]. Rearrangement of Eqs. (1) to (4) gives the coupled TE equations for heat transfer and electric potential as,

$$\rho C\frac{\partial T}{\partial t} + \nabla \cdot (T[\alpha] \cdot \mathbf{J}) - \nabla \cdot ([\lambda] \cdot \nabla T) = \mathbf{E} \cdot \mathbf{J} \tag{5}$$

and

$$\nabla \cdot \left([\varepsilon] \cdot \frac{\partial \phi}{\partial t}\right) + \nabla \cdot ([\sigma] \cdot [\alpha] \cdot \nabla T) + \nabla \cdot ([\sigma] \cdot \nabla \phi) = 0 \tag{6}$$

where $[\varepsilon]$ is the dielectric permittivity matrix [25] and $\mathbf{E}\cdot\mathbf{J}$ represents Joule heat [24].

In Eq. (5), the second term represents the Thomson heat and the third term represents heat transfer due to conduction. In Eq. (6) the first term represents electric current density due to the Seebeck effect and standard voltage driven electric current.

Thermal boundary conditions for (Fig. 1) are as follows;

- The top surface of the TEG experiences constant hot temperature (T_H).
- The bottom surface experiences constant cold temperature (T_C).
- The vertical surfaces of $p-$type and $n-$type are considered with two different conditions: convective heat transfer condition and adiabatic condition (special case).

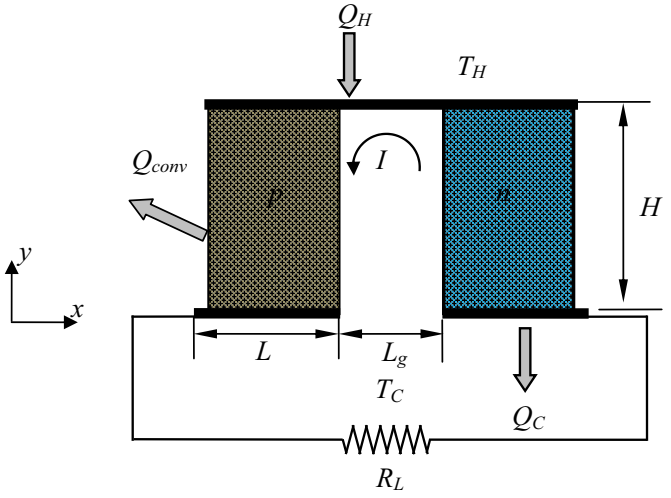

Fig. 1. Schematic of unit cell of TEG.

3. Results and discussion

In this section, the performance of the unit cell of TEG is investigated based on the results obtained by numerically solving governing equations presented in the previous section. For *p*-type material, the nanostructured semiconductor Bismuth Antimony Telluride (*BiSbTe*) is considered to analyze the performance [19]. While for *n*-type material,

Table 1
Polynomial functions of Seebeck coefficient, electrical conductivity, and thermal conductivity as a function of temperature for *BiSbTe* nanostructured bulk alloys and Bi_2Te_3 with *SiC* nanoparticles [19,20].

Properties	Polynomial expressions
α_p	$-139.41 + 1.43T - 5.71 \times 10^{-3}T^2 + 10.71 \times 10^{-6}T^3 - 6.80 \times 10^{-9}T^4$
σ_p	$-338.53 + 7.13T - 2.73 \times 10^{-2}T^2 + 4.15 \times 10^{-5}T^3 - 2.23 \times 10^{-8}T^4$
λ_p	$5.82 - 0.0323T + 1.035 \times 10^{-4}T^2 - 1.61 \times 10^{-7}T^3 + 9.64 \times 10^{-11}T^4$
α_n	$-4.98 \times 10^3 + 47.8T - 1.73 \times 10^{-1}T^2 + 2.73 \times 10^{-4}T^3 - 1.59 \times 10^{-7}T^4$
σ_n	$9.79 - 8.20 \times 10^{-2}T + 3.03 \times 10^{-4}T^2 - 5.05 \times 10^{-7}T^3 + 3.11 \times 10^{-10}T^4$
λ_n	$8.25 - 6.53 \times 10^{-2}T + 2.16 \times 10^{-4}T^2 - 3.22 \times 10^{-7}T^3 + 1.85 \times 10^{-10}T^4$

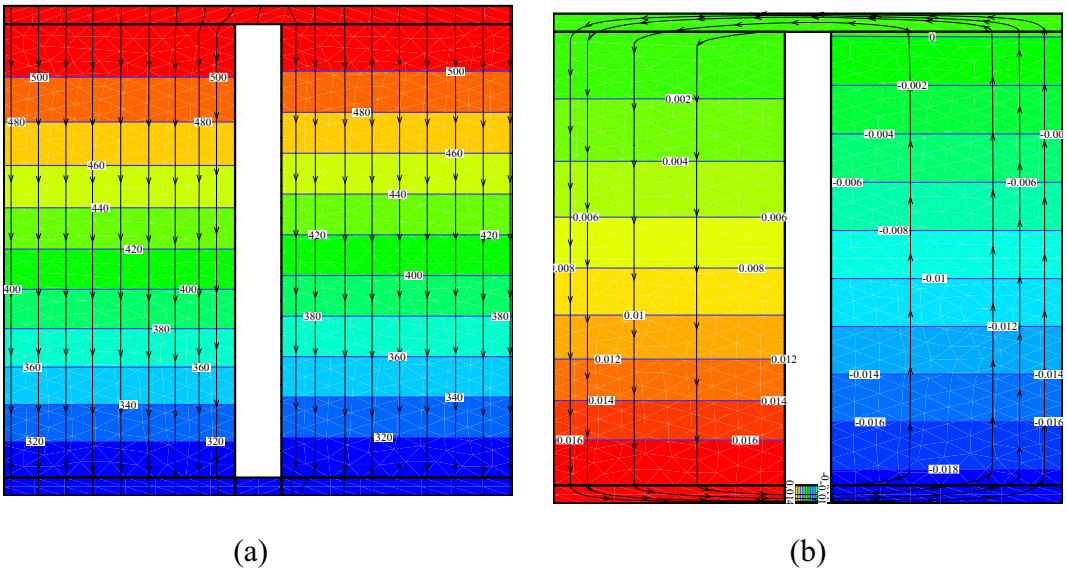

Fig. 2. (a) Contours of heat transfer and (b) contours of electric potential with adiabatic heat transfer condition ($h \approx 0$ W/m^{2}K).

Bismuth Telluride (Bi_2Te_3) with nano-particles of silicon carbide (SiC) is considered to analyze the performance [20]. The temperature dependent transport parameters Seebeck coefficient (α), electrical conductivity (σ), and thermal conductivity (λ) are specified as polynomial functions of temperature as shown in Table 1. These properties are evaluated at an average temperature of working temperature range. The semiconductor leg of unit cell of TEG has dimensions of 1.5 *mm* × 1.5 *mm* and height of 5 *mm*. The gap between two consecutive legs is 0.3 *mm*. The terminals of both *p*-type and *n*-type semiconductor legs are connected with external load (R_L) which are matched with total internal resistance of the TEG. Figs. 2(a), 3(a), 4(a), and 5(a) show field plots of temperature and heat flow. Temperature is presented by marked isothermal lines with multi-colored background, while the heat flow is presented by the vertical lines with arrows. Similarly, Figs. 2(b), 3(b), 4(b), and 5(b) present the field results of electric scalar potential and current flow. The electric potential is indicated by the marked iso-potential lines with multi-colored background, while the current flow is indicated by the lines with arrows. Surface to surrounding convection heat losses are also considered from vertical walls of both semiconductor legs (h = 15–50 W/m^{2}K).

The temperature remains nearly constant at a given location of distance x when convection is absent (i.e., $h = 0$), irrespective of the *p*-type or *n*-type semiconductor leg. However, the location of the same isothermal line is changed in *p*-type and *n*-type legs due to the different transport properties; more specifically, the thermal conductivities. Due to the absence of the surface to surrounding convection, the heat flux lines are parallel in both *p*-type and *n*-type legs and uniformly distributed over the cross-section of the legs. An introduction of the surface to the surrounding convection makes the temperature distribution nonlinear as observed in Figs. 3(a), 4(a), and 5(a). An increment in convection heat transfer coefficient increases the irreversible convection losses through the side walls of semiconductor legs. Higher the convection heat transfer coefficient, more heat is carried away without being converted to electricity. A certain portion of the heat, entering the top

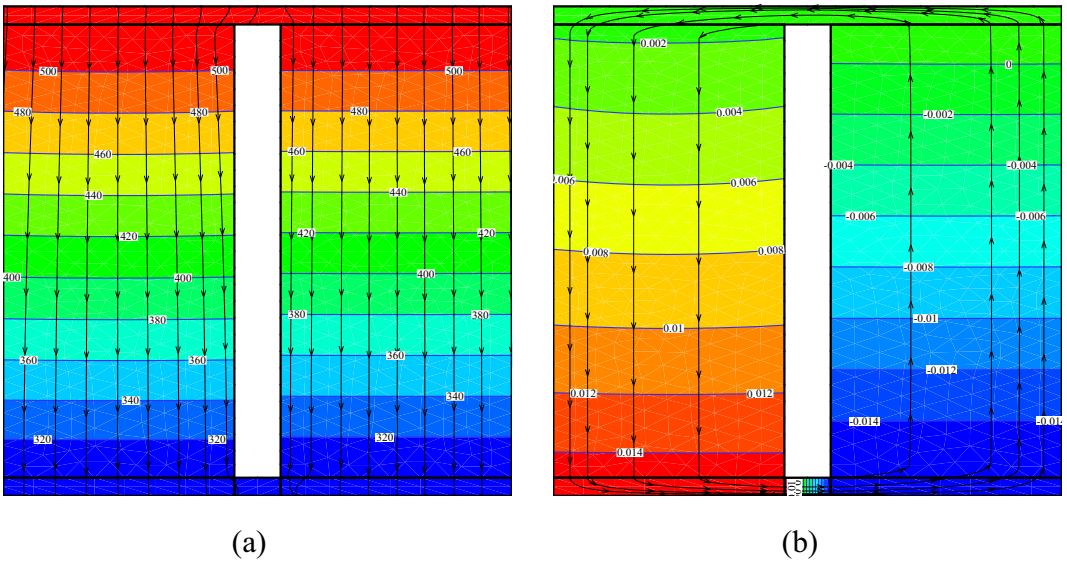

Fig. 3. (a) Contours of heat transfer and (b) contours of electric potential with convective heat transfer boundary condition (h = 15 W/m^{2}K).

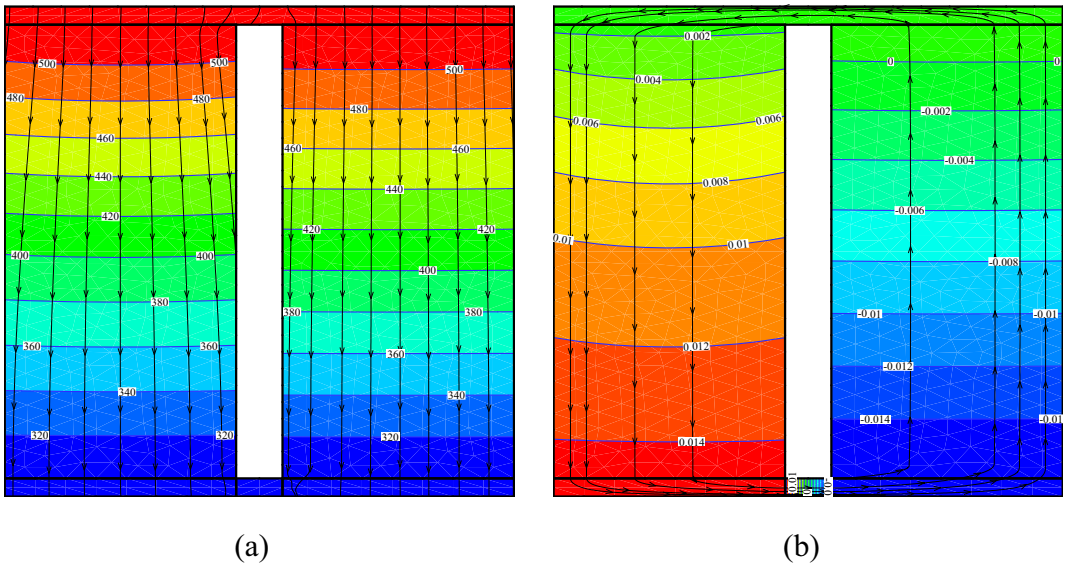

Fig. 4. (a) Contours of heat transfer and (b) contours of electric potential with convective heat transfer boundary condition ($h = 35$ W/m^{2}K).

surface of the TEG, is leaving through the side surfaces by convection as evidenced by the heat flux lines terminated at the vertical side surfaces of the semiconductor legs. The surface of a semiconductor leg is cooler than the core due to the heat removal by convection for a given x location. The heat flux lines are no longer parallel in both p-type and n-type legs and a non-uniform distribution of heat flux line is observed. Due to the coupled thermo-electric effect, a potential difference is established in the TEG which drives an electric current through the system. The electric potential remains nearly constant at a given location of distance x when $h = 0$ for a particular semiconductor leg. However, non-linear electric potential distribution is observed with convective heat transfer boundary condition.

In addition to the numerical simulation, a comparison between analytical result and numerical simulation is presented in terms of the current produced. The analytical results are obtained from the mathematical model developed by Reddy et al. [26]. The comparison is presented in Fig. 6(a) where the produced current is plotted as a function of temperature difference between hot and cold surfaces of the TEG. The electric current increases as temperature difference increases. Fig. 6(a) establishes a good agreement between the current result and result available in the literature. The proposed nanostructured TEG's thermal efficiency is demonstrated in Fig. 6(b) where thermal efficiency is plotted as a function of temperature difference between hot and cold surfaces of the TEG at different values of convection heat transfer coefficients. TEG has highest efficiency with larger temperature difference and adiabatic boundary condition. As convection heat transfer coefficient increases, the thermal efficiency drops and this can be attributed to heat loss shown in temperature field plots from Figs. 3(a), 4(a), and 5(a).

4. Conclusion

In this research paper, a numerical simulation of nanostructured TEG is carried out. The nanostructured TE materials have low thermal conductivity and higher power factor ($\alpha^2\sigma$) which improves the

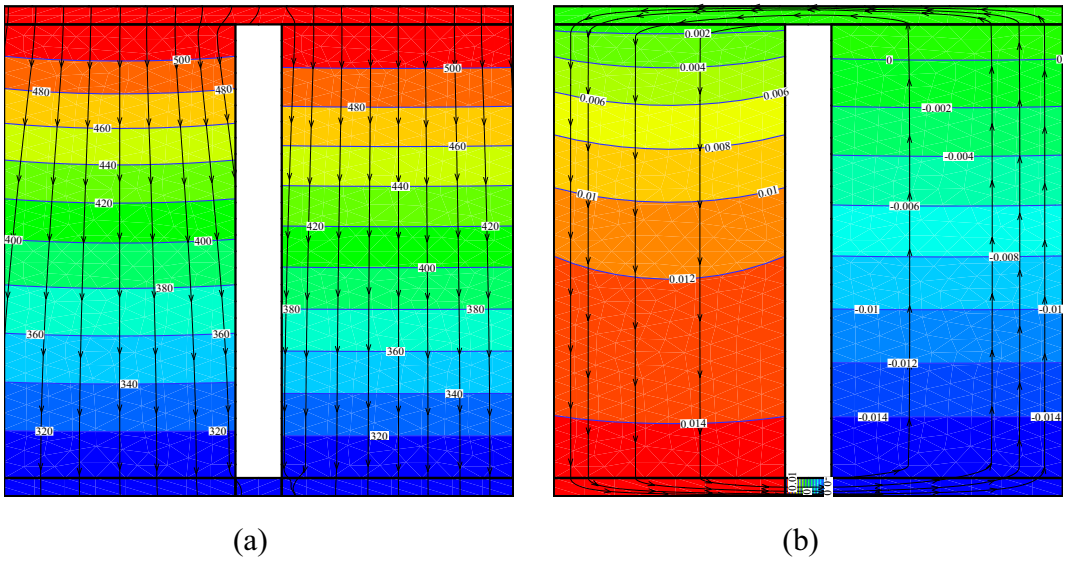

Fig. 5. (a) Contours of heat transfer and (b) contours of electric potential with convective boundary condition ($h = 50$ W/m^{2}K).

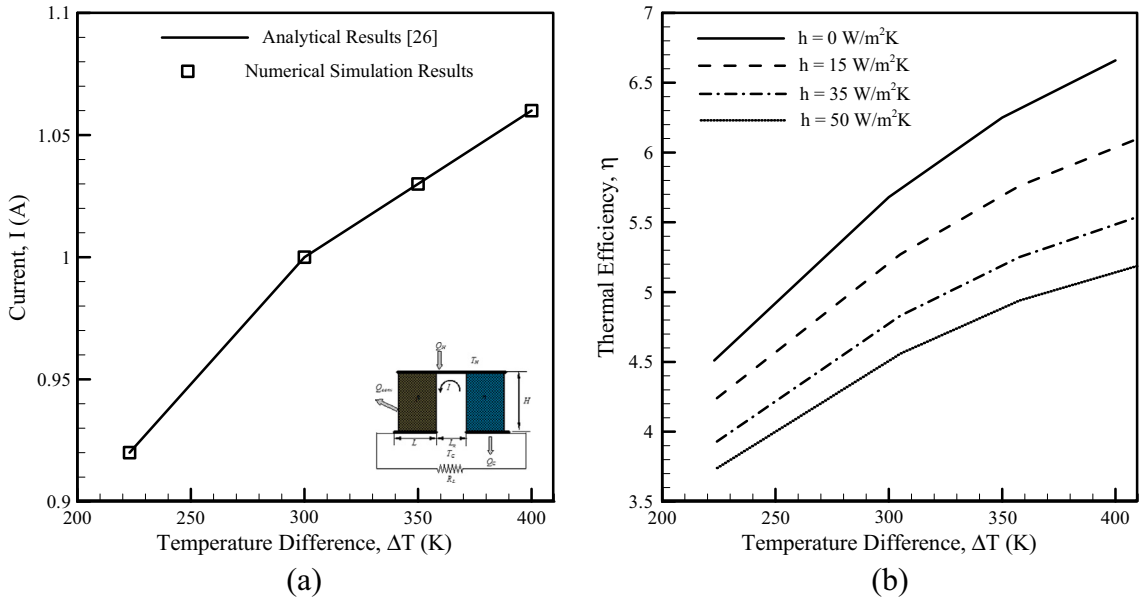

Fig. 6. (a) Comparison of current production using numerical and analytical techniques. (b) Thermal efficiency of TEG as a function of convection heat transfer coefficient and temperature difference.

performance of the TEG. Current numerical simulation considers the Seebeck effect, Peltier effect, Thomson effect, Fourier heat conduction, and convection heat transfer losses. The influences of hot surface temperature and convection heat transfer coefficient on the performance parameters of TEG such as thermal efficiency and electric current have been studied. Electric current generation using numerical simulation and analytical simulation shows a good match. An increase in hot surface temperature leads to increase in electric current generation and eventually the thermal efficiency. Numerical results prove that the presence of irreversible convection heat transfer causes a large amount of heat loss thus reducing the thermal efficiency. In future, more detailed three-dimensional numerical simulation of TEG will be carried out to observe the above mentioned effects in more detail.

Acknowledgment

The authors would like to gratefully acknowledge research grants from Natural Sciences and Engineering Research Council of Canada (NSERC, Grant no. 400495), Ontario Ministry of Agriculture, Food and Rural Affairs (OMAFRA, Grant no. 200370), and School of Engineering Growth Fund, University of Guelph.

References

[1] P. Naphon, S. Wiriyasart, Liquid cooling in the mini-rectangular fin heat sink with and without thermoelectric for CPU, Int. Commun. Heat Mass Transf. 36 (2009) 166–171.
[2] H.S. Huang, Y.C. Weng, Y.W. Chang, S.L. Chen, M.T. Ke, Thermoelectric water-cooling device applied to electronic equipment, Int. Commun. Heat Mass Transf. 37 (2010) 140–146.
[3] O. Sullivan, S. Mukhopadhyay, S. Kumar, M.P. Gupta, Array of thermoelectric coolers for on-chip thermal management, J. Electron. Packag. 134 (2012) 02100501–02100508.
[4] J.C. Wang, Thermoelectric transformation and illuminative performance analysis of a novel LED-MGVC device, Int. Commun. Heat Mass Transf. 48 (2013) 80–85.
[5] Y.Y. Hsiao, W.C. Chang, S.L. Chen, A mathematic model of thermoelectric module with applications on waste heat recovery from automobile engine, Energy 35 (2010) 1447–1454.
[6] A. Rezania, L.A. Rosendahl, S.J. Andreasen, Experimental investigation of thermoelectric power generation versus coolant pumping power in a microchannel heat sink, Int. Commun. Heat Mass Transf. 39 (2012) 1054–1058.
[7] B.V.K. Reddy, M. Barry, J. Li, M.K. Chyu, Thermoelectric performance of novel composite and integrated devices applied to waste heat recovery, Journal of Heat Transfer 135 (2013) 031706.1–031706.11.
[8] X. Gou, H. Xiao, S. Yang, Modeling, experimental study and optimization on low-temperature waste heat thermoelectric generator system, Appl. Energy 87 (2010) 3131–3136.
[9] M. Chen, L.A. Rosendahl, T. Condra, A three-dimensional numerical model of thermoelectric generators in fluid power systems, Int. J. Heat Mass Transf. 54 (2011) 345–355.
[10] B.V.K. Reddy, M. Barry, J. Li, M.K. Chyu, Three-dimensional multiphysics coupled field analysis of an integrated thermoelectric device, Numer. Heat Transf. Part A 62 (2012) 933–947.
[11] S. Zhou, B.G. Sammakia, B. White, P. Borgesen, Multiscale modeling of thermoelectric generators for the optimized conversion performance, Int. J. Heat Mass Transf. 62 (2013) 435–444.
[12] L.L. Baranowski, G.J. Snyder, E.S. Toberer, Concentrated solar thermoelectric generators, Energy Environ. Sci. 5 (2012) 9055–9067.
[13] E. Altenkirch, Elektrothermische kälteerzeugung und reversible elektrische heizung, Phys. Z. 12 (1911) 920–924.
[14] C. Vineis, A. Shakouri, A. Majumdar, M.G. Kanatzidis, Nanostructured thermoelectrics: big efficiency gains from small features, Adv. Mater. 22 (2010) 3970–3980.
[15] G.A. Slack, New materials and performance limits for thermoelectric cooling, in: D.M. Rowe (Ed.), CRC Handbook of Thermoelectric, CRC Press, Boca Raton, Florida, 1995, pp. 407–441.
[16] T.M. Tritt, Thermoelectric materials: principles. Structure, properties, and applications, in: K.H.J. Buschow, R.W. Cahn, M.C. Flemings, B. Ilschner, E.J. Kramer, S. Mahajan, P. Veyssière (Eds.), Encyclopedia of Materials: Science and Technology, Elsevier, 2001, pp. 1–11.
[17] C. Godart, A.P. Gonclaves, E.B. Lopes, B. Villeroy, Role of structures on thermal conductivity in thermoelectric materials, in: V. Zlatic, A. Hewson (Eds.), Properties and Applications of Thermoelectric Materials, Springer, Dordrecht, The Netherlands, 2009, pp. 19–49.
[18] Y. Ma, R. Heijl, A.E.C. Palmqvist, Composite thermoelectric materials with embedded nanoparticles, J. Mater. Sci. 48 (2013) 2767–2778.
[19] B. Poudel, Q. Hao, Y. Ma, Y. Lan, A. Minnich, B. Yu, X. Yan, D. Wang, A. Muto, D. Vashaee, X. Chen, J. Liu, M.S. Dresselhaus, G. Chen, Z. Ren, High-thermoelectric performance of nanostructured bismuth antimony telluride bulk alloys, Science 320 (2008) 634–638.
[20] L.D. Zhao, B.P. Zhang, J.F. Li, M. Zhou, W.S. Liu, J. Liu, Thermoelectric and mechanical properties of nano-*SiC*-dispersed Bi_2Te_3 fabricated by mechanical alloying and spark plasma sintering, J. Alloys Compd. 455 (2008) 259–264.
[21] H. Li, X.F. Tang, Q.J. Zhang, C. Uher, High performance $In_xCe_yCo_4Sb_{12}$ thermoelectric materials with insitu forming nanostructured InSb phase, Appl. Phys. Lett. 94 (2009) 10211401–10211413.
[22] D. Kraemer, B. Poudel, H. Feng, J.C. Caylor, B. Yu, X. Yan, Y. Ma, X. Wang, D. Wang, A. Muto, K. McEnaney, M. Chiesa, Z. Ren, G. Chen, High-performance flat-panel solar thermoelectric generators with high thermal concentration, Nat. Mater. 10 (2011) 532–538.
[23] K. McEnaney, D. Kraemer, Z. Ren, G. Chen, Modeling of concentrating solar thermoelectric generators, J. Appl. Phys. 110 (2011) 0745021–0745026.
[24] J.L. Perez-Aparicio, R. Palma, R.L. Taylor, Finite element analysis and material sensitivity of Peltier thermoelectric cells coolers, Int. J. Heat Mass Transf. 55 (2012) 1363–1374.
[25] L.D. Landau, E.M. Lifshitz, L.P. Pitaevskii, Electrodynamics of Continuous Media, Second ed. Butterworth-Heinemann, Burlington, MA, 1984.
[26] B.V.K. Reddy, M. Berry, J. Li, M.K. Chyu, Thermoelectric performance of novel composite and integrated devices applied to waste heat recovery, J. Heat Transf. 135 (2013) 0317061–03170611.